DEPARTMENT OF ELECTRICAL ENGINEERING
INDIAN INSTITUTE OF TECHNOLOGY MADRAS
CHENNAI – 600036

Explorations with Fibre Lasers

A project report

Submitted by

PANKAJ KUMAR DAS

in partial fulfilment of requirements for the award of the degree

Of

MASTER OF TECHNOLOGY

June 2022

THESIS CERTIFICATE

This is to undertake that the project report titled **EXPLORATIONS WITH FIBRE LASERS**, submitted by me to the Indian Institute of Technology Madras, for the award of **MASTER OF TECHNOLOGY** (Photonics) in Electrical Engineering, is a bona fide record of the research work done by me under the supervision of **Dr. Anil Prabhakar**. The contents of this project report, in full or in parts, have not been submitted to any other Institute or University for the award of any degree or diploma.

Chennai 600036 **Pankaj Kumar Das**

Date: June 2022

Dr. Anil Prabhakar
Research Guide
Professor
Department of Electrical Engineering
IIT Madras

ACKNOWLEDGEMENTS

I express my sincere gratitude to Prof. Anil Prabhakar, Professor, Department of Electrical Engineering, Indian Institute of Technology, Madras who have been constant sources of inspiration and guidance throughout the execution of my this project.

I would like to thank Debanuj Chatterjee(Project associate) and Gautam Shaw(PhD scholar) his assistance in carrying out the experiments safely and numerous pedagogical discussions and additional mention of Ashutosh Singh for his help in taking out experimental readings and plots.

ABSTRACT

KEYWORDS Ytterbium doped optical amplifiers, thermo-optic effect, Ring laser, Fabry-Perot filter, Erbium doped fiber, BER, EDFA, Link Design

In the optical fiber presence of high power induces non-linear effects and similarly in high power fiber laser presence of high power further induce thermo-optic effect along with non-linear effect. Thermo-optic effect brings modification in refractive index profile. Once the refractive index profile changes eigenmodes are no longer orthogonal to each other and mixing of modes results in power transfer among the modes of the fiber. The objective of the project is to simulate the consequences of thermo-optic effect on fiber modes and modal instabilities at the output through an algorithm which implement the physics of a high power fiber laser working using python and its tool.

Second part of the project is to build a stable ring laser comb. Ring laser comb is very useful in situation where multiple channel/source is required like four wave mixing to generate entangled photon pair from HNLF. Bit error rate tells about how many bits are wrongly received in comparison to transferred bits and hence it measures the data integrity in a communication link

CONTENTS

LIST OF TABLES

LIST OF FIGURES

ABBREVIATIONS

ASE Amplified Spontaneous Emission.

BER Bit Error Rate.

EDF Erbium Doped Fiber.

EDFA Erbium Doped Fiber Amplifier.

FPF Fabry-Perot Filter.

HNLF Highly Non-linear Fiber.

OSA Optical Spectrum Analyzer.

WDM wavelength division multiplexing.

CHAPTER 1

THERMAL INSTABILITIES IN HIGH POWER FIBER LASERS

1.1 INTRODUCTION

Presence of high power in fiber lasers can induce non-linear and thermo-optic effect which changes the temperature inside the fiber and it results in modification of the refractive index of the fiber. Our aim is to simulate the consequence of thermo-optic effect in the fiber modes and its modal instabilities.

1.2 PARAMETERS USED IN SIMULATION

Dimensions of the fiber	Length of the fiber(L) Core radius(r_0) Inner clad radius(r_1) Outer clad radius(r_2)	1.5 m 37 μm 85 μm 200 μm
Wavelength	Signal wavelength(λ_s) Pump wavelength(λ_p)	1064 nm 977 nm
Relative Permittivity Values	ϵ_{core} $\epsilon_{\text{Inner-clad}}$ $\epsilon_{\text{Outer-clad}}$	2.0745 2.0740 2.0736
Thermal Coefficients	Core thermal conductivity(k_0) Thermo-optic Coefficient($\frac{dn}{dT}$)	1.38 $W/m-K$ 1.2e-5 $/K$
Lasers Parameters	Signal emission cross-section(σ_{es}) Signal absorption cross-section(σ_{as}) Pump emission cross-section(σ_{ep}) Pump absorption cross-section(σ_{ap}) Spontaneous relaxation time(τ) Yb+ Dopant concentration(N_{ion})	3.58e-25 m^2 6.00e-27 m^2 1.87e-24 m^2 1.53e-24 m^2 850 μs 3.5e25 m^{-3}

1.3 ALGORITHM

Our model uses beam propagation method along with steady-state thermal solver to study these phenomena along the length of the fiber. The model works in saturation

regime, in presence of thermal induced grating simulates self-focusing and gain saturation, and coupling of the perturbed modes. In this model a grid of 383×383 dimension is created to solve the steady-state 2D-thermal equation and mode equation in the core is solved for a truncated grid 95×95 using Eigen solver from **scipy.sparse.linalg** package. Since speed of light is much higher than thermal diffusion hence rate calculation can be done for multiple times before a thermal calculation. Here we have taken 40 optical step between two thermal calculation.

1.3.1 Scalar Wave Equations

$$\Delta^2 E(x, y, z) + n^2(x, y, z) k_0^2 E(x, y, z) = 0 \qquad Keiser\ (2010) \tag{1.1}$$

where $k_0 = \frac{\omega}{c}$, free space vector, n(x, y, z) is the refractive index profile and E(x, y, z) is the electric field distribution.

Invoking slowly varying envelope and paraxial approximation, we get

$$[-2i\beta \frac{\partial}{\partial z} + \Delta_t^2 + n^2(x, y, z) k_0^2 - \beta^2] E^2(x, y, z) = 0 \tag{1.2}$$

Here, β is the wave vector responsible for oscillations of the wave in propagation direction and Δ_t is the transverse Laplacian Operator. Assuming slow variation in electric field along z direction, we have

$$\frac{\partial^2}{\partial x^2} + \frac{\partial^2}{\partial y^2} + n^2(x, y) k_0^2] E(x, y) = \beta^2 E(x, y) \tag{1.3}$$

Applying FDM(finite difference method) and taking $\Delta x = \Delta y$, we get

$$\begin{aligned} &\frac{E(x + \Delta x, y) + E(x, y + \Delta y) + E(x - \Delta x, y) + E(x, y - \Delta y)}{\Delta x^2} \\ &\qquad - \frac{4E(x, y)}{\Delta x^2} + n^2(x, y) k_0^2 E(x, y) = \beta^2 E(x, y) \end{aligned} \tag{1.4}$$

The above equation could be converted into matrix form as $Ax = \lambda x$ which is solved using eigen solver(eigs) to find first three eigenvalues $\beta 1$, $\beta 2$, $\beta 3$ and corresponding eigenvectors $e_1(x, y)$, $e_2(x, y)$, $e_3(x, y)$. $e_i(x, y)$ are normalized electric field corresponding to i^{th} mode of the fiber. $e_1(x, y)$ is the fundamental and the other two are

first higher order degenerate modes, here other higher order modes are not included considering negligible power in those modes.

1.3.2 Power Profile

$$P_{si}(x, y, z_0) = P_i(z_0)|e_i(x, y, z_0)|^2 \tag{1.5}$$

where $P_{si}(x, y, z_0)$ is the signal profile, $P_i(z_0)$ is the total power and $e_i(x, y, z_0)$ is the normalized electric field for i^{th} mode of the fiber at $z = z_0$

1.3.3 Gain and Heat generation

Assuming uniform Pump signal in core cross-section due to very small cross-section compare to inner-clad cross-section, we can write pump intensity as

$$I_p(x, y, z_0) = \frac{P_{\text{pump}}(z_0)}{Area_{\text{inner-clad}}} \tag{1.6}$$

and signal intensity in the presence of three wave can be written as

$$I_s(x, y, z_0) = \frac{|\sum_{i=1}^{3} \sqrt{P_i(z_0)} e_i(x, y, z_0) e^{j\beta_i z_0}|^2}{\Delta x \Delta y} \tag{1.7}$$

Fiber core is an active region which is considered to be uniformly doped with Yb^{3+} Ion.Two level rate equation is assumed and incoming pump and signal photon with enough energy takes ion from GND state to excited state band.

The excited ion population is given by

$$\frac{dN_2}{dt} = \sigma_{ap}\phi_p N_1 + \sigma_{as}\phi_s N_1 - \sigma_{ep}\phi_p N_2 - \sigma_{es}\phi_s N_2 - \frac{N_2}{\tau} \quad Chenet\ al.\ (1992) \tag{1.8}$$

At steady state $\frac{dN_2}{dt} = 0$, solving we get

$$N_2(x,y,z_0) = N_{tot}(x,y,z_0) \frac{\frac{I_s(x,y,z_0)\sigma_{as}}{h\nu_s} + \frac{I_p(x,y,z_0)\sigma_{ap}}{h\nu_p}}{\frac{1}{\tau} + \frac{(\sigma_{as}+\sigma_{es})I_s(x,y,z_0)}{h\nu_s} + \frac{(\sigma_{ap}+\sigma_{ep})I_p(x,y,z_0)}{h\nu_p}} \tag{1.9}$$

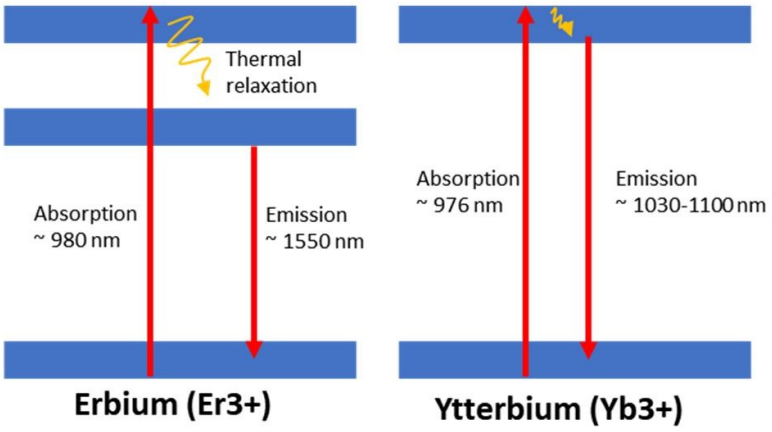

Figure 1.1: Energy state of $Yb^{3+}ion$

Then, the ground state population is given by

$$N_1(x, y, z_0) = N_{tot}(x, y, z_0) - N_2(x, y, z_0) \tag{1.10}$$

Assumption - Negligible attenuation and scattering losses, gain for the signal and pump is given by

$$g_s(x, y, z_0) = \sigma_{es} N_2(x, y, z_0) - \sigma_{as} N_1(x, y, z_0) \tag{1.11}$$

$$g_p(x, y, z_0) = \sigma_{ep} N_2(x, y, z_0) - \sigma_{ap} N_1(x, y, z_0) \tag{1.12}$$

Power profile of i^{th} mode after propagating dz length, changes to

$$P_{si}(x, y, z_0 + dz) = P_{si}(x, y, z_0)(1 + g_s(x, y, z_0)dz) \tag{1.13}$$

Total power in i^{th} mode is given by

$$P_i(z_0 + dz) = \iint P_{si}(x, y, z_0 + dz)\, dx\, dy \tag{1.14}$$

Pump power evolution after propagating dz length is given by

$$P_{\text{pump}}(z_0 + dz) = P_{\text{pump}}(z_0) + \iint \{I_p(x, y, z_0) g(x, y, z_0) dz\}\, dx\, dy \tag{1.15}$$

Excited ion undergoes non-radiative relaxation and comes down to lower energy band releasing thermal energy. Heat is calculated at the end of optical(gain) calculation cycle(neglecting the contribution from spontaneous emission) is given by

$$Q(x,y,z_0+k*dz)=(\frac{\nu_p}{\nu_s}-1)\{I_s(x,y,z_0+k*dz-I_s(x,y,z_0)\} \tag{1.16}$$

where, k is the number of optical-step between two thermal calculation.

1.3.4 Steady-state Heat Equation

The steady-state heat equation with heat source in homogeneous medium is a Poisson's equation, given by

$$\Delta^2 T(x,y,z_0) = \frac{-Q(x,y,z_0)}{k_0} \tag{1.17}$$

where Q is the heat source and k_0 is the thermal conductivity of the core. We have Dirichlet boundary condition in x and y direction and considering thermal diffusion in radial direction but not in propagation direction since boundary(heat sink) is closer than the propagation length. Assuming free convection as less efficient and only considering heat dissipation from optical fiber via conduction, thermal equation can be re-written as

$$\frac{\partial^2 T(x,y,z_0)}{\partial x^2} + \frac{\partial^2 T(x,y,z_0)}{\partial y^2} = \frac{-Q(x,y,z_0)}{k_0} \tag{1.18}$$

Applying FDM, we get

$$\begin{aligned} \frac{T(x+\Delta x,y,z_0)+T(x-\Delta x,y,z_0)-2T(x,y,z_0)}{\Delta x^2} + \frac{T(x,y+\Delta,z_0)}{\Delta y^2} \\ + \frac{T(x,y-\Delta y,z_0)-2T(x,y,z_0)}{\Delta y^2} = \frac{-Q(x,y,z_0)}{k_0} \end{aligned} \tag{1.19}$$

We iteratively solve above 2D-heat equation to arrive at true $T(x,y,z_0)$ from which $\Delta T(x,y,z_0)$ is obtained.

1.3.5 Thermo-Optic Effect

The increment in Temperature profile by $\Delta T(x, y, z_0)$ modifies the refractive index profile for the next iteration as following -

$$n^2(x, y, z_0 + k * dz) = n_{rt}^2 + 2n_{rt}\frac{dn}{dT}\Delta T(x, y, z_0) \tag{1.20}$$

where n_{rt} is the refractive index profile at room-temperature equivalent to $n(x, y, z = 0)$, k is the number of optical step and $\frac{dn}{dT}$ is the thermo-optic coefficient.

1.3.6 Overlap Integrals

The change in refractive index due to change in temperature is considered as perturbation and hence the modes will also change according to change in refractive index which again can be calculated from scalar wave equation. As the mode changes, power transfer between different happens which depends upon overlap factor as

$$\Gamma_{ij} = \frac{|\iint e_i(x, y, z_0 + dz)e_i(x, y, z_0 + dz)\, dx\, dy|^2}{\iint |e_i(x, y, z_0)|^2\, dx\, dy \; * \iint |e_i(x, y, z_0)|^2\, dx\, dy} \tag{1.21}$$

Power transfer in i^{th} modes is given by

$$P_i(x, y, z_0 + dz) = \sum_{j=1}^{3} \Gamma_{ij}\, P_i(x, y, z_0) \tag{1.22}$$

These steps is again repeated along the length z of the fiber and power evolution of signal and pump is noted neglecting scattering or any other kind of loss and also negligible line-width of the lasers are considered.

1.4 OBSERVATION & CONCLUSION

The results added here, has been taken after multiple try & change in the simulation parameter to arrive at correct results. 40 optical step(4mm) has been taken between two thermal calculation. The results provides us the comparison in output in presence and absence of thermo-optic effect. The results added here, has been taken after multiple try & change in the simulation parameter to arrive at correct results. 40 optical step(4mm)

has been taken between two thermal calculation. The results provides us the comparison in output in presence and absence of thermo-optic effect.

1.4.1 Space step convergence

Gain equation for pump is given by $e^{-\alpha_p dz}$ and for fairly small value of dz exponential gain could be written as $-\alpha_p dz$. So smaller the dz step smoother the propagation. see fig. 4.5

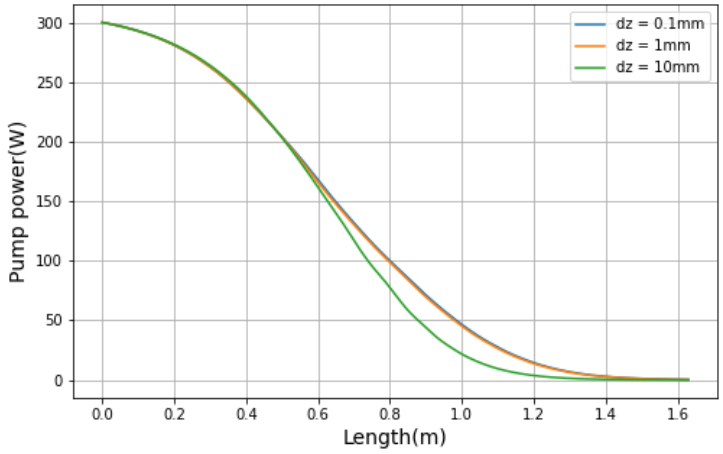

Figure 1.2: Pump power is plotted against different dz, and as we can see for dz = 0.1mm and 1mm the curves are overlapping and considering smooth propagation dz = 0.1mm is chosen

1.4.2 Comparison between thermal solver

This simulation is done with two different methods of thermal solver to validate the accuracy of thermal solver. We first used iterative method to arrive at true temperature profile of the cross-section and it was taking 95% of the simulation time. As thermal calculation limits the speed performance of the program, we converted the cross-section into a matrix and used inbuilt **spsolver** from scipy.sparse.linalg package to compute temperature profile and it improved the speed significantly with negligible error in temperature calculation. see table 1.2

1.4.3 Future Scope

This model assumes steady state for thermal calculation but transient model is necessary to modal temporal fluctuations in the output beam due to thermo-optic effect. Thermal calculation limits the speed of the simulation so implementing GPU programming, speed could be improved further. In this model we compute eigenmodes of the fiber at every step which keeps rotating due to symmetry of the fiber and if that is fixed then accuracy in estimating overlap integrals would be better and hence overall outputs.

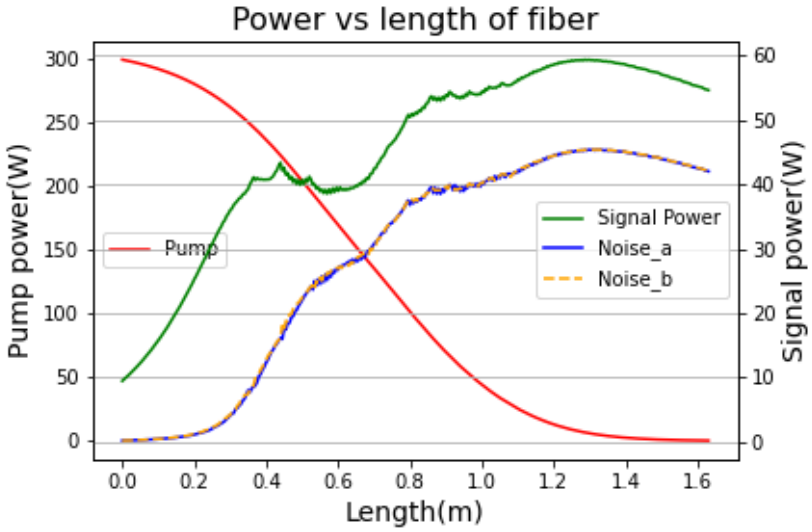

Figure 1.3: Power propagation in pump and different modes of the fiber in presence of thermo-optic effect, Signal power goes from 9.5 W to 55 W and 1st Higher order modes power changes from 0.25 W to 42 W. see table C.1

Power in	Input	Without thermo-optic effect	With thermo-optic effect
Fundamental mode	9.5 W (95%)	270 W (93.75%)	55 W (**39.6**%)
Higher-order mode	0.5 W (5%)	18 W (6.25%)	84 W (**60.4**%)
Ratio (FM:HOM)	19	15	**0.655**

Table 1.1: Power shared by different modes at the end of the fiber.

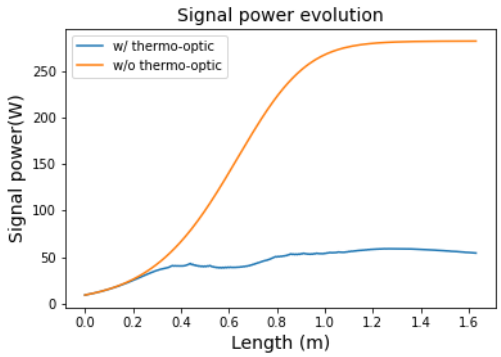

Figure 1.4: This plot compare the gain achieved by signal in presence and absence of the thermo-optic effect

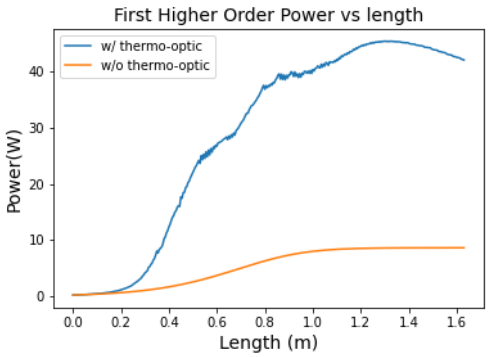

Figure 1.5: First higher order mode gains significant power due to power transfer from signal in presence of thermo-optic effect

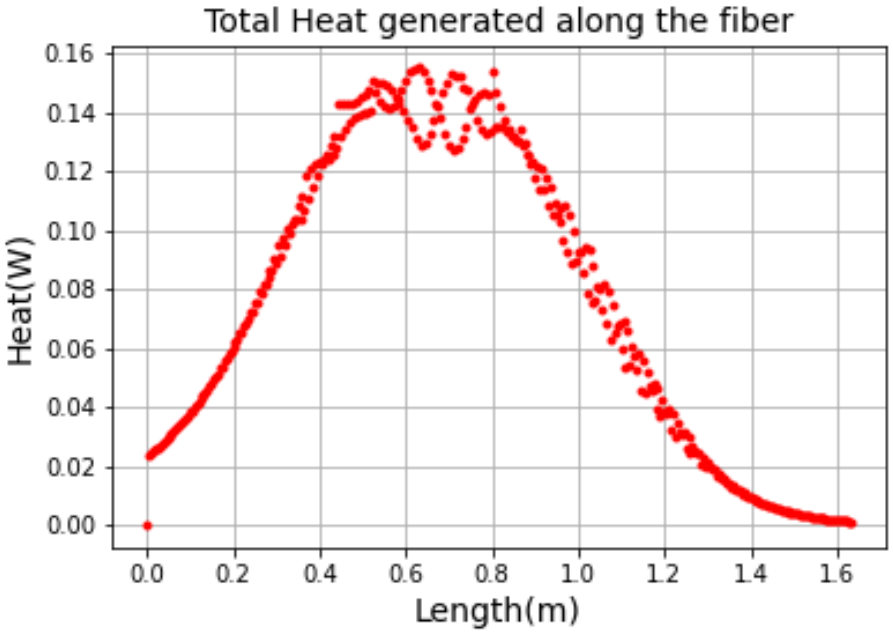

Figure 1.6: Total heat generated at every 5mm step of the fiber, it is observed that maximum heat is generated at 0.6-0.8 mm where maximum rise in refractive index had occurred

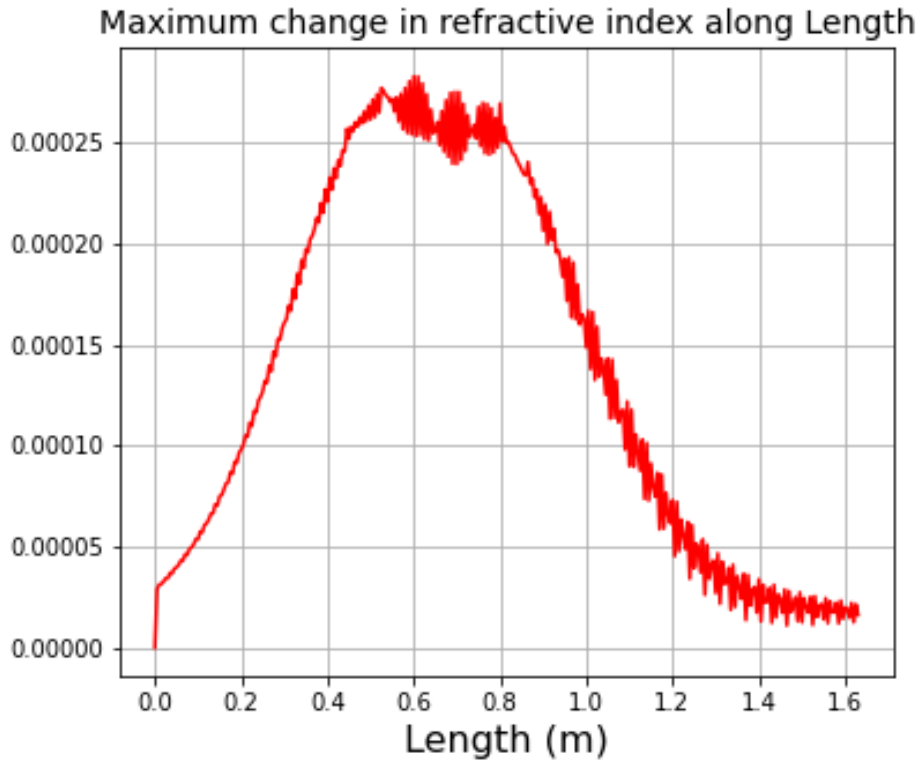

Figure 1.7: When excited atoms relaxes to meta-stable state, heat is released which raises the temperature hence refractive index also increases with positive change in temperature

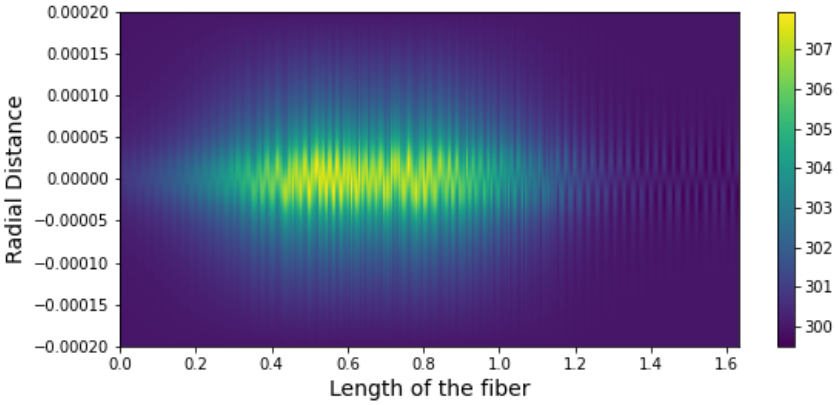

Figure 1.8: Heat is generated in the core hence temperature is initially increasing there but after sufficient decrease in pump power it slowly comes to normal condition, Note: radial distance is in um and length is in m

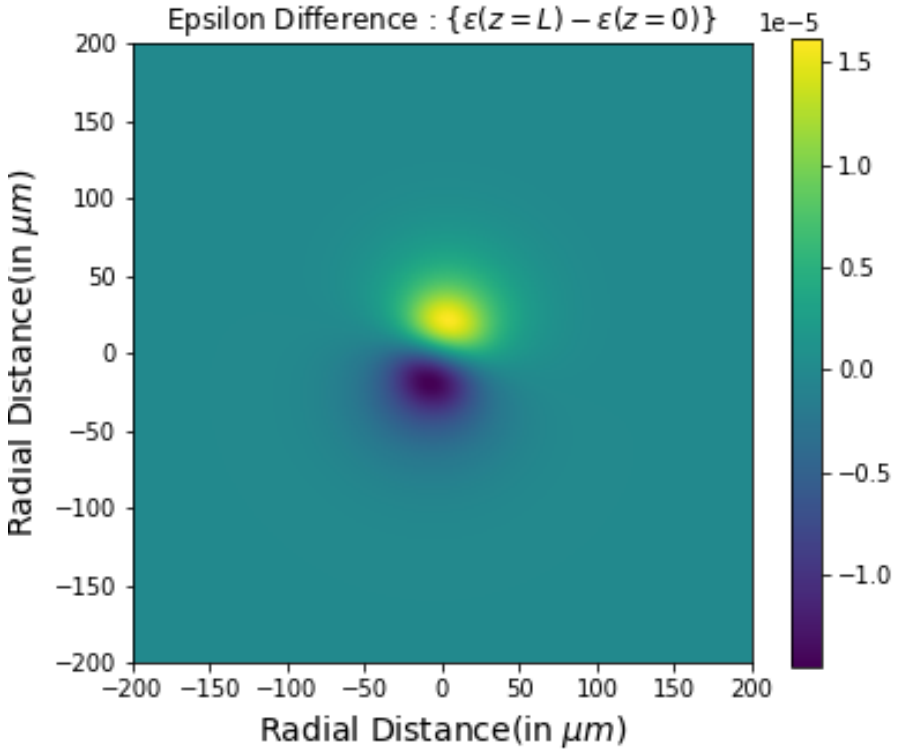

Figure 1.9: Maximum change in ϵ_r at the two end of the fiber is at the centre which implies self focusing of the beam, we can see two spots of both +ve and -ve change in ϵ_r which could have accumulated due to matrix rotation of mode at every thermal step calculated (yet to be verified)

Methods→ Outputs↓	Temperature convergence upto an error 1e-6	Temperature convergence upto an error 1e-7	Temperature calculation with spsolver
Time taken for each step	(0.11-0.20) mins	(0.10-1.52) mins	**(1.55-1.65)secs**
Total simulation time	38.14 mins	5.26 hrs	**12.25 mins**
Total heat generated	24.72 W	24.72 W	**24.70 W**

Table 1.2: Comparison of thermal solver, first two columns shows time taken for temperature converging iteratively and last column is the time taken in estimating temperature profile through solving Poisson heat equation using spsolver package

CHAPTER 2

EDF CHARACTERISATION

2.1 INTRODUCTION

Optical fiber is doped with rare earth material like Erbium ion work as an amplifier. Erbium ion has three set of states and when it is pumped the ground state ions goes to excited state and hence it acts as a source for stimulated emission.

2.2 EDF CHARACTERIZATION

As a first step to build the ring laser, we need to characterize the EDF that we are using. The characterization is classified into three experiments : to check the EDF's forward and backward ASE spectra, to see the gain response of the EDF when it acts as an amplifier, and to compare the forward and the backward ASE spectra.

2.2.1 EDF ASE Spectra

We check the output ASE spectra of the EDF with an OSA for different pump powers. The scheme for this experiment is shown in Fig.2.1.

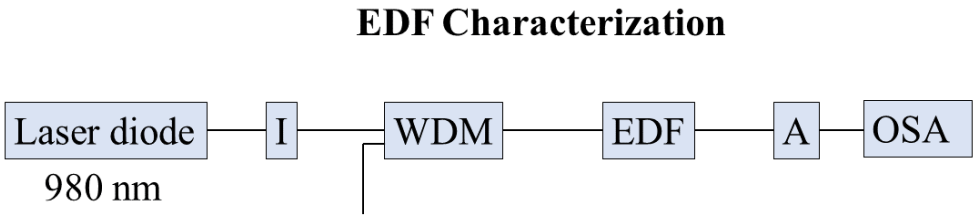

Figure 2.1: Experimental scheme to observe the EDF spectra for different pump currents (powers).

The EDF output spectra for different pump powers are shown in Fig. 2.6 (b). As expected, we clearly see the 1530 nm peak of the EDF and with increasing pump powers and the

vertical shift of the spectra stops once the medium gets saturated.

2.2.2 EDF Gain

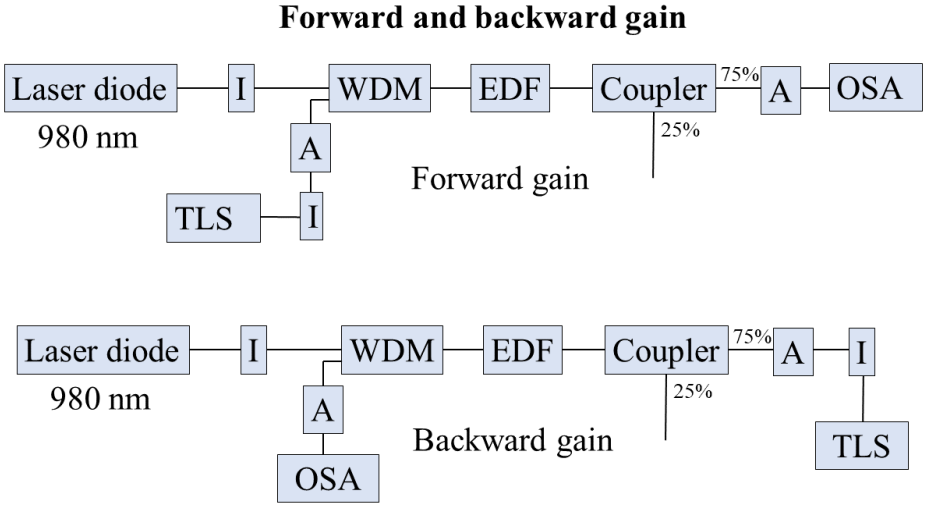

Figure 2.2: Experimental scheme for forward and reverse pumping configuration

Fiber core is doped with three level energy system erbium ion which when interacts with pump photon undergoes population inversion. This population inversion creates stimulated emission for incoming signal photon and hence work as an amplifier. To estimate the gain offered by the medium to different input signal for various pump power in forward and reverse pumping configuration we setup an experiment as shown in fig. 2.2. We observe that for lower pump power reverse pumping configuration provides slightly more gain than that of forward pumping possibly due to the reason that in forward pumping signal photon immediately encounters highly inverted channel and many of stimulated photon gets reabsorbed while in reverse pumping stimulation happens gradually. For higher pump power gain is the same because of saturation.

2.2.3 Comparison of Forward and Backward ASE

Spontaneous emission happens in all direction and as it passes through the medium it gain some power due to population inversion and we observe amplified version of it at the two end of the fiber. From fig 2.6 we infer that spontaneous emission is random as

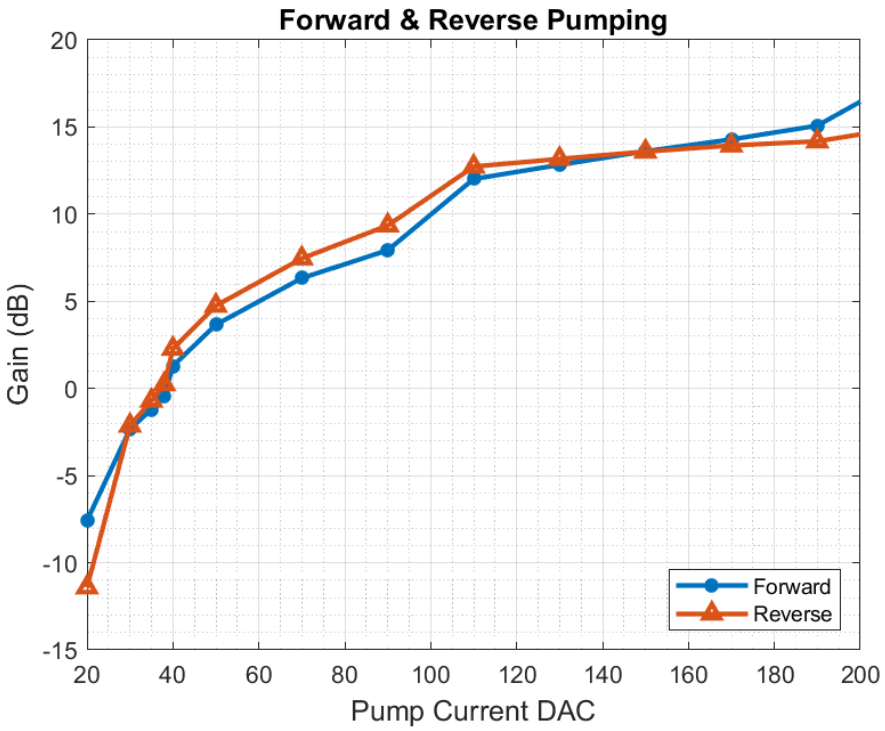

Figure 2.3: Gain characterisation of edf for forward and backward pumping

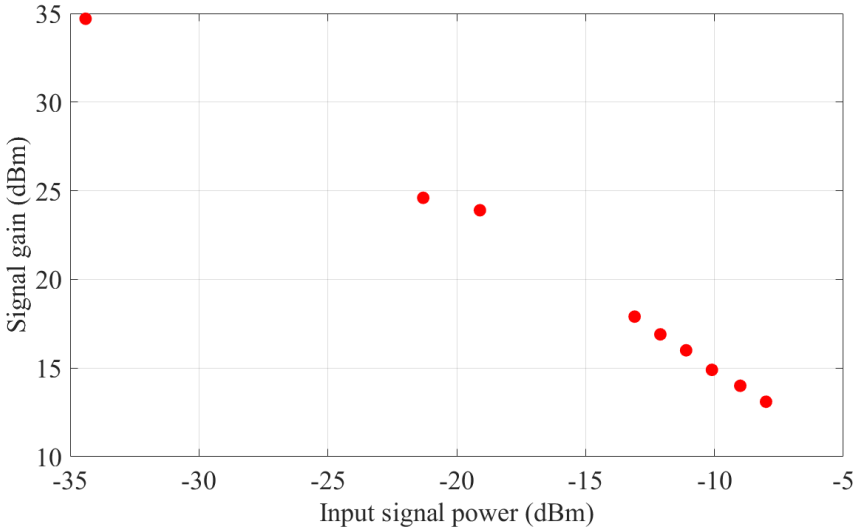

Figure 2.4: Gain of input signal as a function of input signal power.

the spectrum observed at the two end are similar, we also can see that power in backward ASE are slightly more than the forward ASE since the backward ASE encounters higher pump power at the start of the fiber.

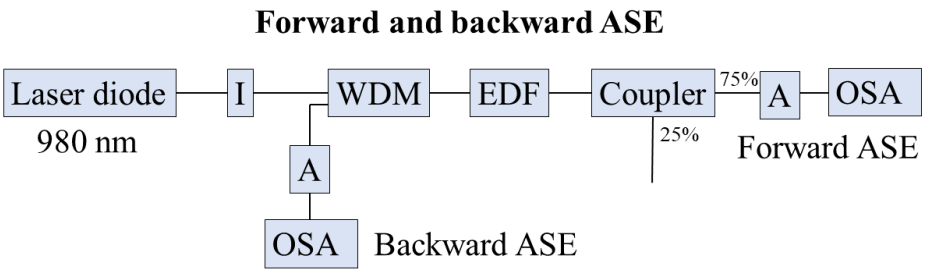

Figure 2.5: Experimental scheme to observe the forward and backward ASE of the EDF.

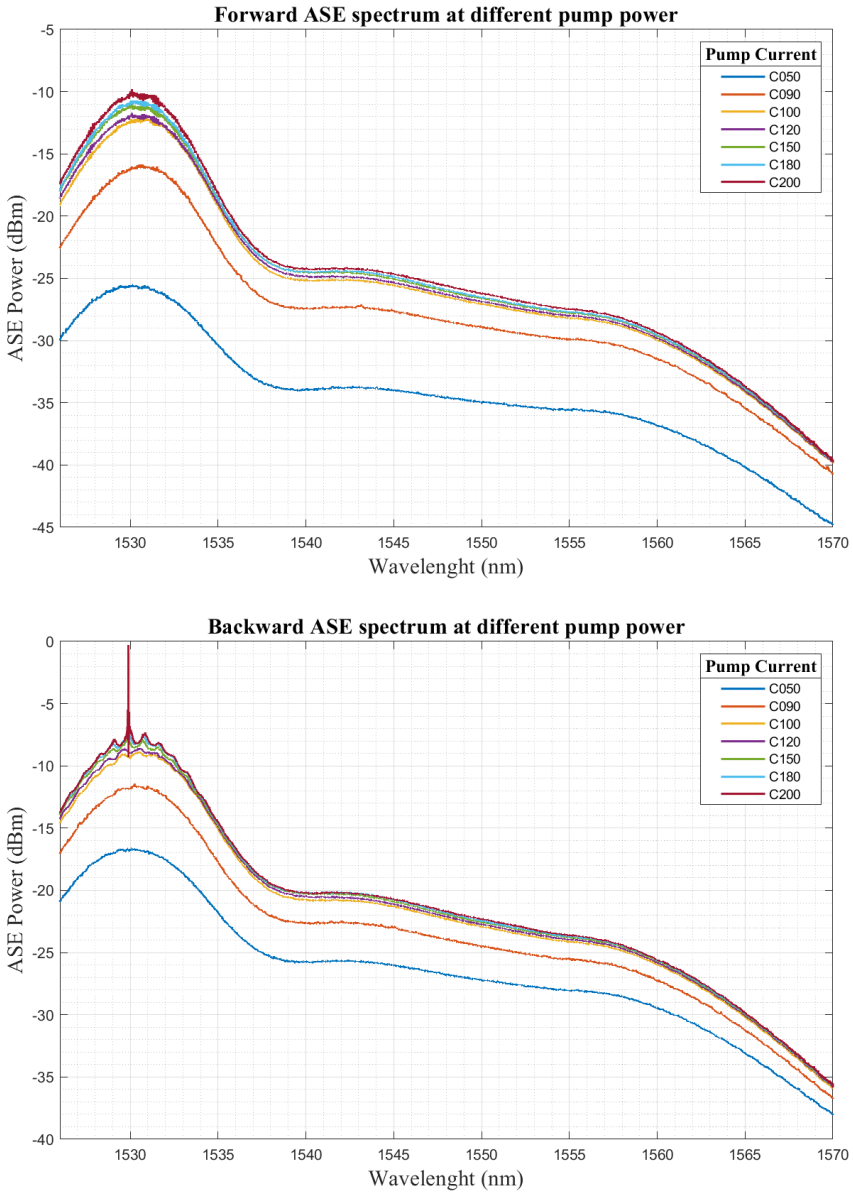

Figure 2.6: Forward (a) and backward (b) ASE spectra of the EDF.

CHAPTER 3

RING LASER USING FPF

3.1 INTRODUCTION

The operation principle of the ring laser scheme as shown in Fig. 3.1 is as follows. A laser diode at 980 nm acts as a pump and pumps the gain medium, which in our case is the EDF. The emission of the Er atoms happens around 1560 nm and is fed back into the ring using a WDM coupler. The output is tapped out from the 25% port of a 75:25 coupler.

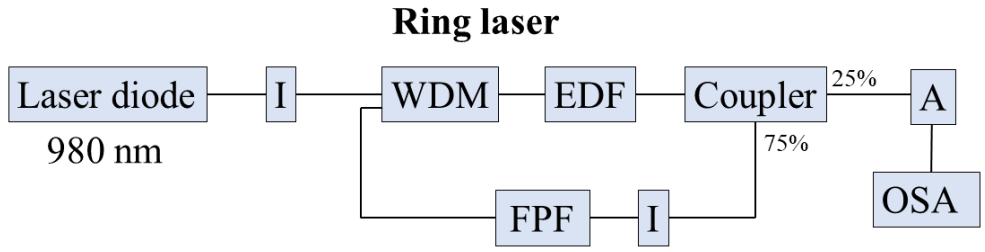

Figure 3.1: Scheme of a ring laser with an EDF and a FPF in the ring. The 980 nm laser diode acts as the pump. I : Isolator, A : Attenuator

3.2 COUPLING RATIO OF COUPLER

3.2.1 Numerical Determination of Coupling Ratio

One can understand that for achieving lasing from a ring laser, the gain and loss of the cavity in one round trip should balance each other. Now we can see from the scheme in Fig. 3.1, the amount of optical power that is allowed to remain in the ring in each cavity round trip, is determined by the coupling ratio of the coupler. Obviously, a high coupling ratio (like 99:1 where 99% is fed back into the ring) will lead to feeding back a large input to the ring and hence the gain of that input will be easily saturated by the EDF.

While on the other extreme, a very low coupling ratio (like 1:99) will lead to a small signal even after an amplification by the EDF, and hence the power in the ring will keep decreasing after every round trip, until it becomes zero. Thus to have a stable power circulating in the ring, the coupling ratio needs to be chosen optimally, such that there is a balance between the gain and the loss in the ring.

From the previously discussed Section 2.2 about the EDF characterization, we acquired the information about how the gain G provided by the EDF to an input signal changes as a function of the input signal power P_{in} and the pump power P. In our case, we chose a pump power of 250 mW, where we have already seen that the EDF gain is saturated. In fact the EDF gain gets saturated above 200 mW of pump power. In such a case, the power that is fed into the ring in the n-th round trip $P_{in,n}$, is given by the recursion :

$$P_{in,n} = P_{in,n-1} G(P_{in,n-1}) x, \tag{3.1}$$

where x is the coupling ratio that goes into the ring. $G(P_{in})$ was found by fitting a second order polynomial with the experimental data for signal gain as a function of the input signal power for 250 mW input pump power (see blue curve in Fig. 3.2). From the fit, we

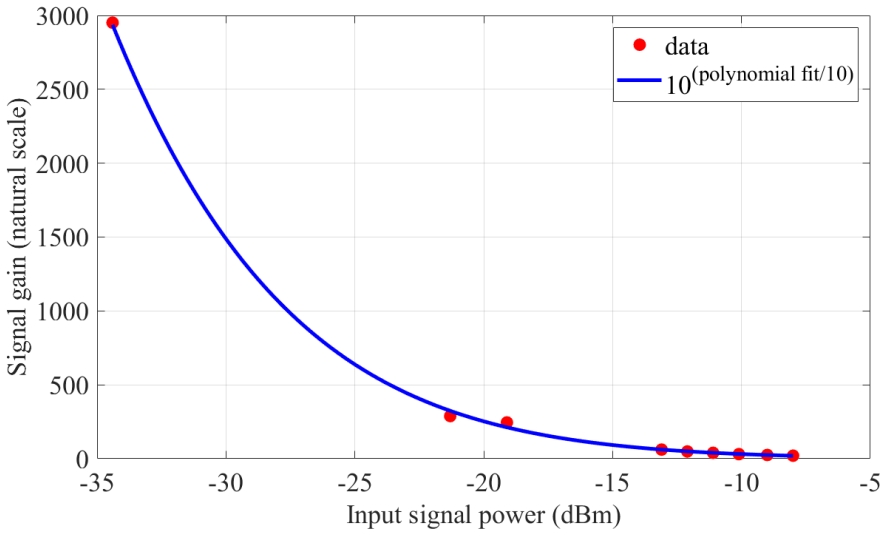

Figure 3.2: Gain of input signal (in natural scale) as a function of input signal power (in dBm). A second order polynomial fit is shown in blue.

get the dependence of G (in natural units) on P_{in} as :

$$G = 10^{(0.0069P_{in}^2 - 1.1124P_{in} + 4.5222)/10}. \tag{3.2}$$

After running this iteration over 10 cycles, we determined the stable value of P_{in} in the ring. We also verified that for different starting values of P_{in}, $P_{in,n}$ always asymptotically converged to the same value after large ($\sim n$ =10) number of iterations. In Fig. 3.3 we show the stable output power of the ring $P_{in}(1-x)$ as a function of the coupling ratio x. From Fig. 3.3 we see that a value of x near 0.5 leads to the maximum output of the

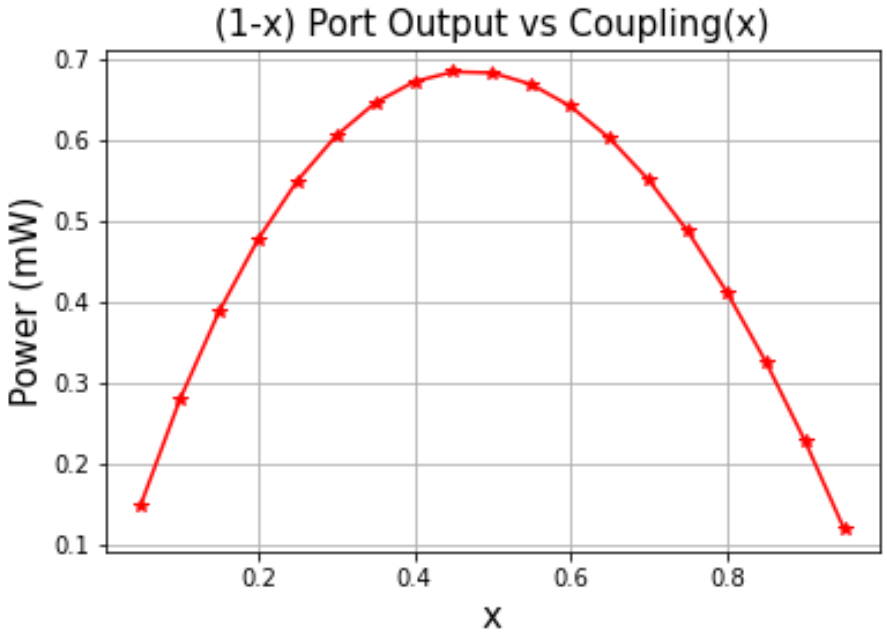

Figure 3.3: Plot of $P_{in}(1-x)$ vs coupling ratio x.

ring laser. Thus we acquired a coupler with coupling ratio $x = 0.65$ which was close to the optimal value of 0.5. However before using it we also determined its x-value experimentally and it turns out to be 0.75 (see appendix: C for coupler characterisation).

3.3 FPF CHARACTERIZATION

In order to characterize the FPF, we used the scheme shown in Fig. 3.4. The FPF we used has a comb shaped transmission and the comb can be shifted in wavelength by applying

a voltage across it. It should be noted here that the FPF has a maximum input power of

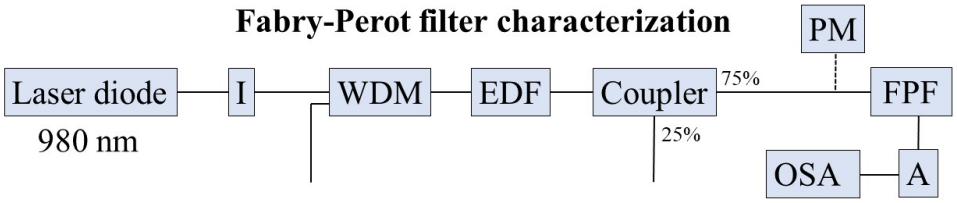

Figure 3.4: Experimental setup for Fabry-Perot Filter characterisation

60 mW and the voltage applied across it can vary from 0 V to 12 V for its safety and optimal operation. Thus we ensured the power falling on the FPF is always less than 50 mW (21 mW in our case) and varied the voltage across it (0 V, 5 V and 10 V) to see the filtered ASE using an OSA. The spectra for different voltages is shown in Fig. 3.5, where we can clearly see the shift of the comb lines.

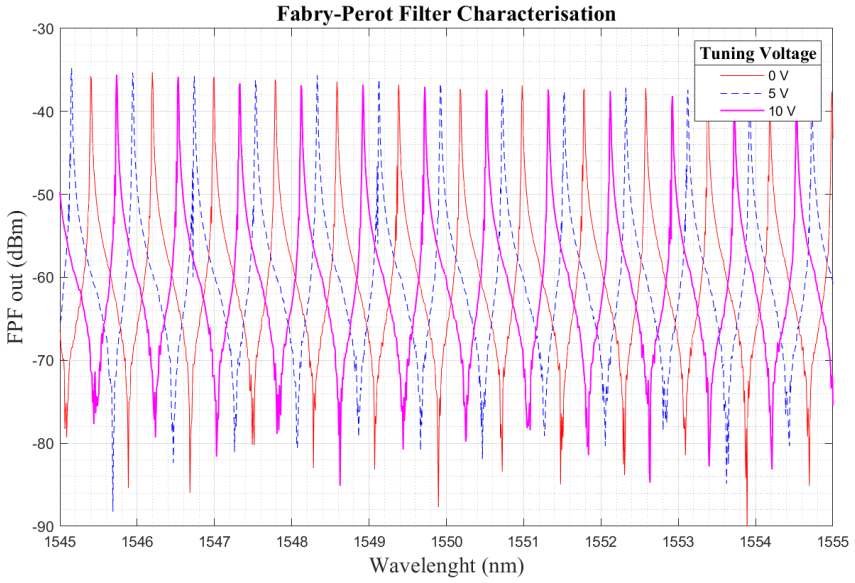

Figure 3.5: Output spectra of the FPF for different voltages applied across the FPF.

3.4 RING LASER

Having performed all the required characterizations we finally make the ring in the setup (see Fig. 3.1). To form a ring configuration we connect the 75% port output of the coupler to the WDM input through a FPF with an isolator connected in series to prevent backward power flow in the ring. We observe the output spectra of the ring laser from the 25% output port using an OSA.

In Fig. 3.6a we can see only one mode lasing for the lower pump power but two mode(in line with FPF peak, spacing 0.8 nm 3.6b) lasing for the higher pump power. This is because for a higher pump power, the cavity has enough power to sustain two modes. We expect to achieve more lasing modes with even higher pump powers.

3.5 SUMMARY

To conclude, we discussed about the characterization for different components required for building a ring laser based on a EDF cavity. We inserted an FPF inside the cavity to select out certain frequencies for lasing. Finally we observed the lasing at two different wavelengths near 1560 nm. The lasing peaks were separated by 0.8 nm, which was the comb line spacing of the FPF. We can use a different FPF with a comb spacing of 0.4 nm to get a larger number of comb lines in the ring laser emission.

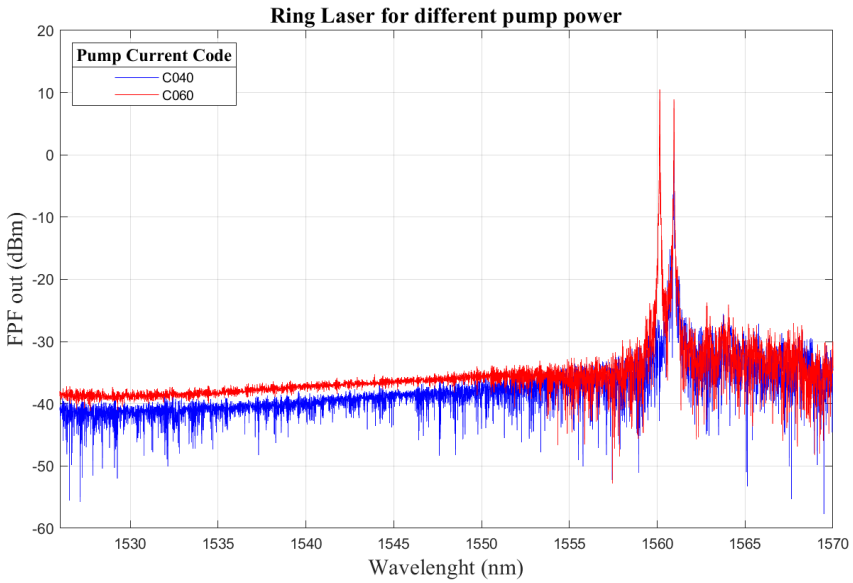

(a) Lasing Mode around 1560 nm

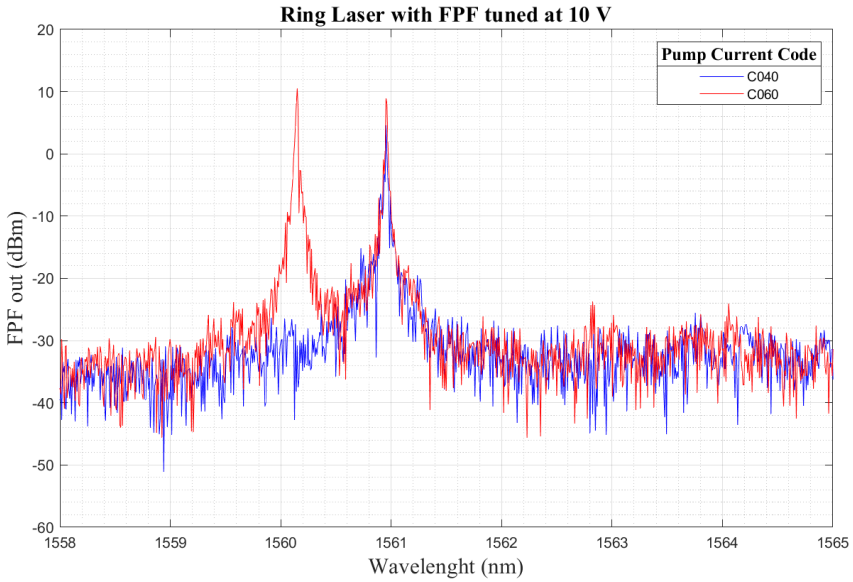

(b) Zoomed version of (a)

Figure 3.6: Output spectra of the ring laser for different pump currents (DAC current input C040(blue) & C060(red)

CHAPTER 4

STABILIZING RING LASER COMB WITH EDFA

4.1 EDFA CHARACTERIZATION

We are using an in-line EDFA for amplifying and stabilising the ring laser output peaks. The idea here is to provide enough gain to all the peaks such that they saturate and provide a stable output power. So we first characterised the gain of the EDFA by varying the input signal power at 1550 nm using the scheme mentioned in Fig. 4.1. This EDFA amplifies higher input signals less and vice versa (see Fig. 4.2). We use an attenuator before the EDFA to ensure the input power to the EDFA is below 10 dBm as 10 dBm is the maximum input power EDFA could take.

In the ring laser we generated peaks at different wavelengths and these peaks are separated by 0.4 nm due to the FPF in the ring. In the Fig. 4.3 we can see that for higher input powers, *i.e* 0 dBm, the EDFA amplifies all the wavelengths roughly to 15 dBm, but for lower input powers, the output varies from 10 dBm to 12 dBm.

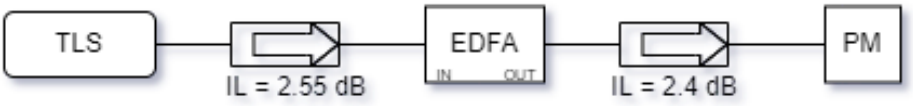

Figure 4.1: Scheme used for gain and spectrum characterisation of Optilab in-line EDFA. Isolators are connected for TLS and EDFA's pump laser safety.

4.2 RING LASER ANALYSIS

We operate the Ring laser shown in Fig. 4.4 at 185 mW pump power because the output are clean with the power periodically exchanging among the 5 peaks shown in the

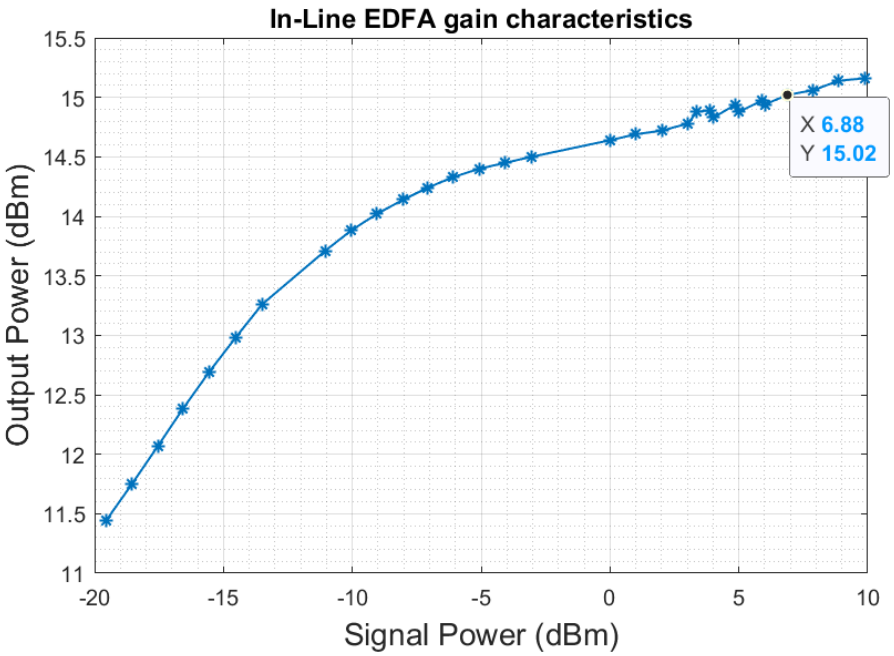

Figure 4.2: Gain characteristic of the EDFA.

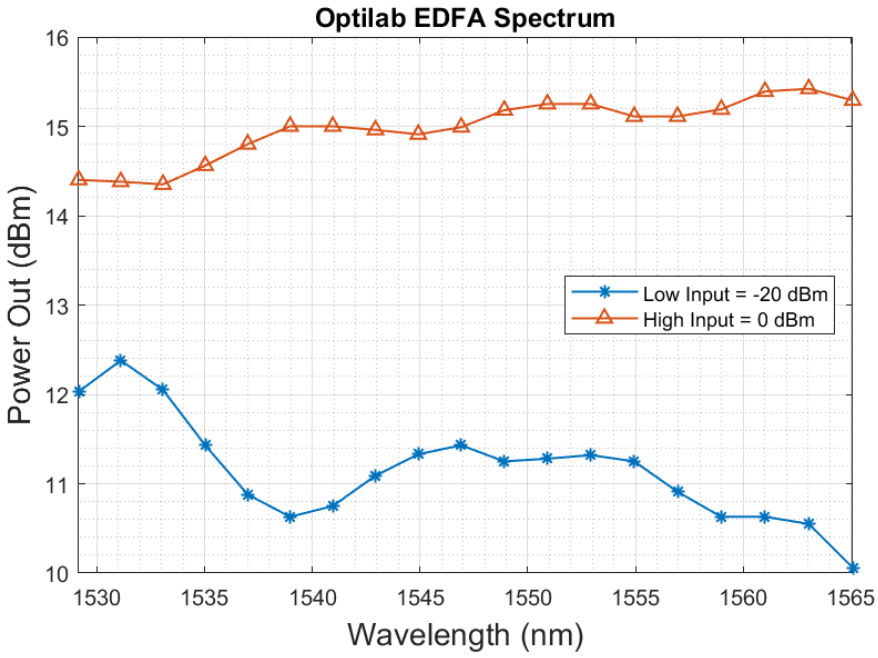

Figure 4.3: Spectrum of EDFA output power for low and high input signal powers.

spectrum 4.6. Since the spectrum is periodically changing we take 10 sample spectrum at the output(25 % port of the coupler), averaged it to represent the output spectrum of

the ring laser (see Fig. A.4 for the spectrum). We read the output power in the power meter, it is 17.5 dBm, but the peaks are not stable so we pass this spectrum through the in-line EDFA as it could amplify the smaller peaks and stabilize the peaks further. Peaks at the output of the EDFA were behaving similarly as it was at the input of EDFA, *i.e* output from the ring laser.

4.2.1 Peak Detection

Since the peak were not stable and changing often, we took multiple spectra sample to do the statistical analysis (like mean power and standard deviation in power of each peaks). We removed the higher frequency/noise from the average spectrum as shown in Figs. 4.5 and 4.6. It smoothed the spectrum and now it was easy to pick the peaks from both the spectra. Fig. A.4 shows the peak analysis of the ring laser output and we can see the mean peak power varying from 6.3 mW to 16 mW and its standard deviation varying from 4.3 mW to 8.3 mW. In Fig. A.3 we show the analysis for the amplified ring laser, where we can see the standard deviation being below 1.7 mW in each peaks. This suggest that the peaks are around its mean power. So we can say that the EDFA does provide some stability to the lasing peaks and this was also visible on the computer screen via the OSA.

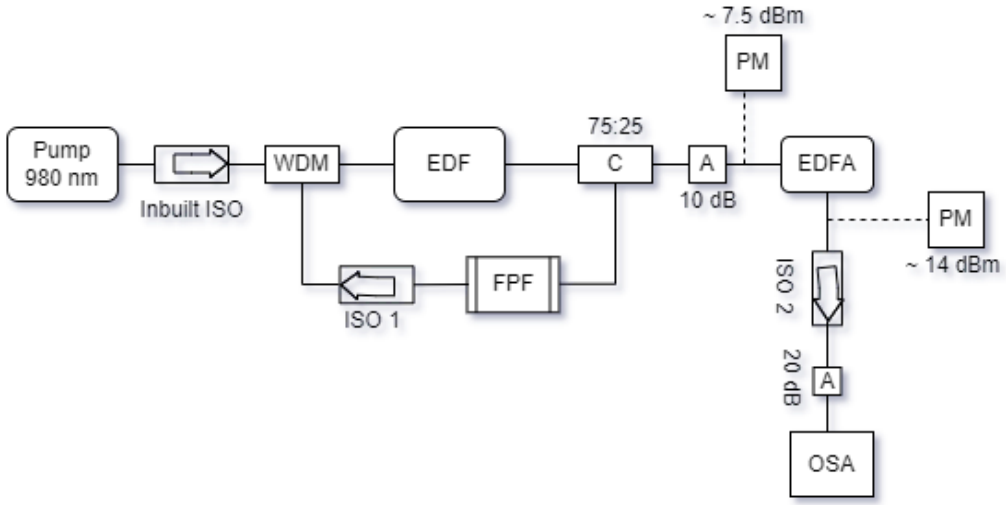

Figure 4.4: Experimental setup used for amplifying ring laser output using an EDFA.

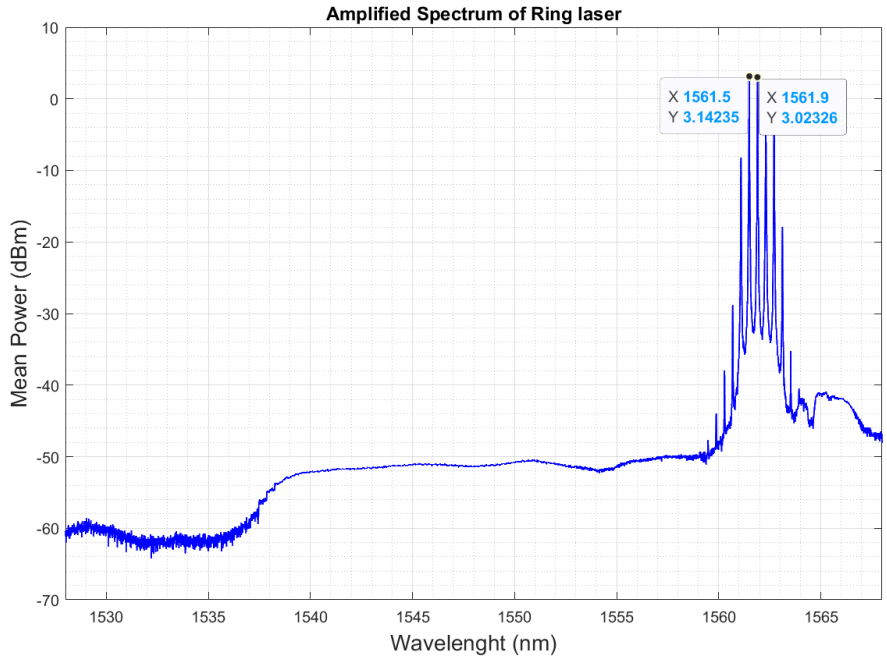

Figure 4.5: Averaged spectrum of EDFA output.

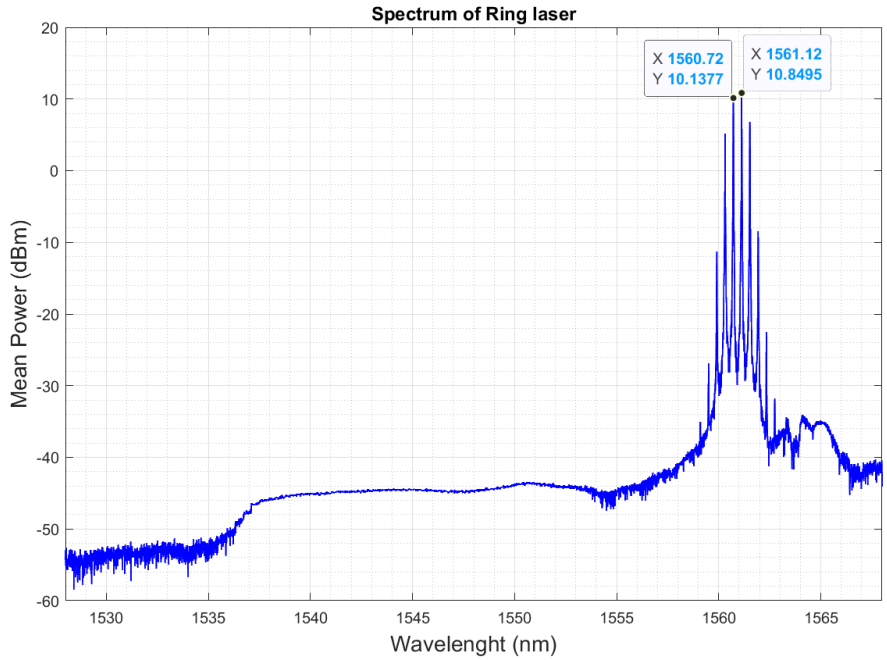

Figure 4.6: Averaged spectrum of ring laser.

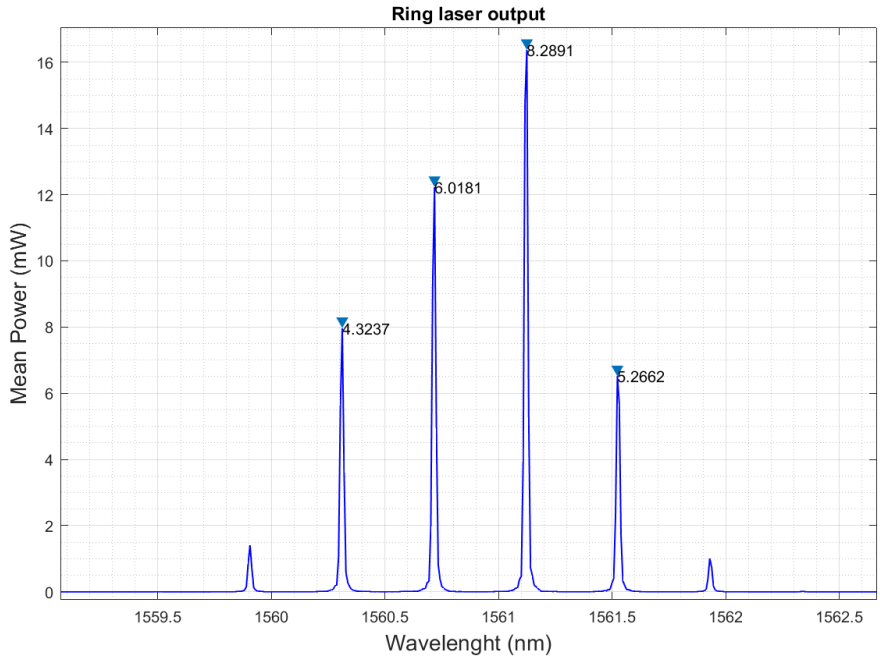

Figure 4.7: Lasing modes of Ring laser on a linear scale. Standard deviation in each peaks are put above it.

4.3 OBSERVATION

At the 25 % port output of the coupler we have ≈ 17.5 dBm power but the EDFA can take only upto 10dBm as input, so this power is attenuated with a 10 dB attenuator and fed ≈ 7.5 dBm into EDFA and the output was around 14 dBm, i.e 3 dBm less than the ring laser output. Output of the EDFA is advised to be connected through an isolater. The isolater 2 has insertion loss of 2.4 dB. This further weakened the EDFA output and now it was weaker.

4.4 CONCLUSION

We stabilized the ring laser output comb to some extent using the EDFA but overall power of the comb dose not change by much.

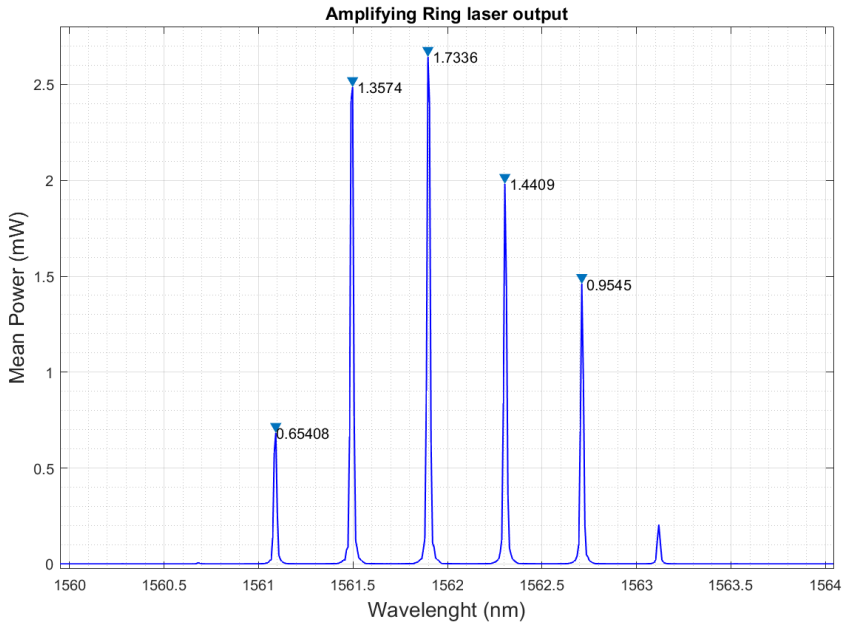

Figure 4.8: EDFA output on linear scale. Standard deviation of each peaks are shown above it.

CHAPTER 5

BER PERFORMANCE

5.1 INTRODUCTION

We use EDFA for amplifying the signal every 80 km in a typical communication link. EDFA also adds noise according to the receiver bandwidth to the signal which needs to be estimated before establishing a proper functioning communication link.

5.2 ABOUT OPTOBERT DEVICE

OptoBERT device has BER analyser for electrical signal and so we use an XFP to convert optical signal to electrical signal. XFP's laser have centre wavelength of 1550.12nm and transmit signal at 0 dBm power and supports 9.95Gb/s to 11.3Gb/s bit rates. After passing through 30 km fiber received signal strength is -5.52 dBm which is well above receiver responsivity -16 dBm. refer figure 5.1(a).

5.3 BER MEASUREMENT

OptoBERT device we use here to analyse the BER performance of point to point 30km link and the effect of amplifier in a link. We see how BER changes with varying pump power for different modulated signal at 10Gbps data rate.

5.3.1 P2P 30 km fiber link

In the point to point 30 km fiber link modulated signal transferred with 0 dBm power at 10 Gbps data rate. For PRBS7, PRBS31 and 1010... user pattern the BER is high while BER is zero for 1100... user pattern, see table 5.3. Once we change the user pattern from 1010... to 1100... the On-Off time got doubled i.e. time period is doubled now and hence the data rate is halved. So in a direct P2P link the BER is only affect by dispersion which

is highly dependent on the data rate hence we see better BER performance for 1100.... pattern signal.

5.3.2 BER measurement across EDF

Refer to figure 5.1(b) scheme, for the effect of EDF on BER first before adding it in the link. Same SFP at 10 Gbps data rate is used here and a Power meter is connected to 25% output port of the coupler to read the power at the output of the EDF before connecting to the detector(receiver) for its safety and maintaining the received power around -6 dBm via connecting required attenuator. BER get worse with increasing pump power due to ASE noise, refer to table 5.1. Higher pump power is avoided as ASE noise increases non-linearly as the power increase in comparison to signal power which saturates eventually and hence it further worsens the BER performance.

5.3.3 BER performance after adding EDFA in the link

After adding the EDFA in the link we see a significant change in the BER performance as the signal strength is increased and after passing through 30 km ASE power decreases by -6 dBm making the overall signal to noise power ratio better. BER get worse with increasing pump power as it should since the ASE power increases non-linearly with pump power and it gets better decreasing the dispersion but ASE always dominates the BER performance. Refer to table 5.2 for the recorded data.

Sequence	Pump Power	BER
PRBS7	C100	5.97E-05
	C150	2.01E-03
PRBS31	C100	7.08E-03
	C150	7.52E-03
1010 1010... 32bit seq	C100	2.68E-04
	C150	4.62E-03

Table 5.1: BER measurement after amplification

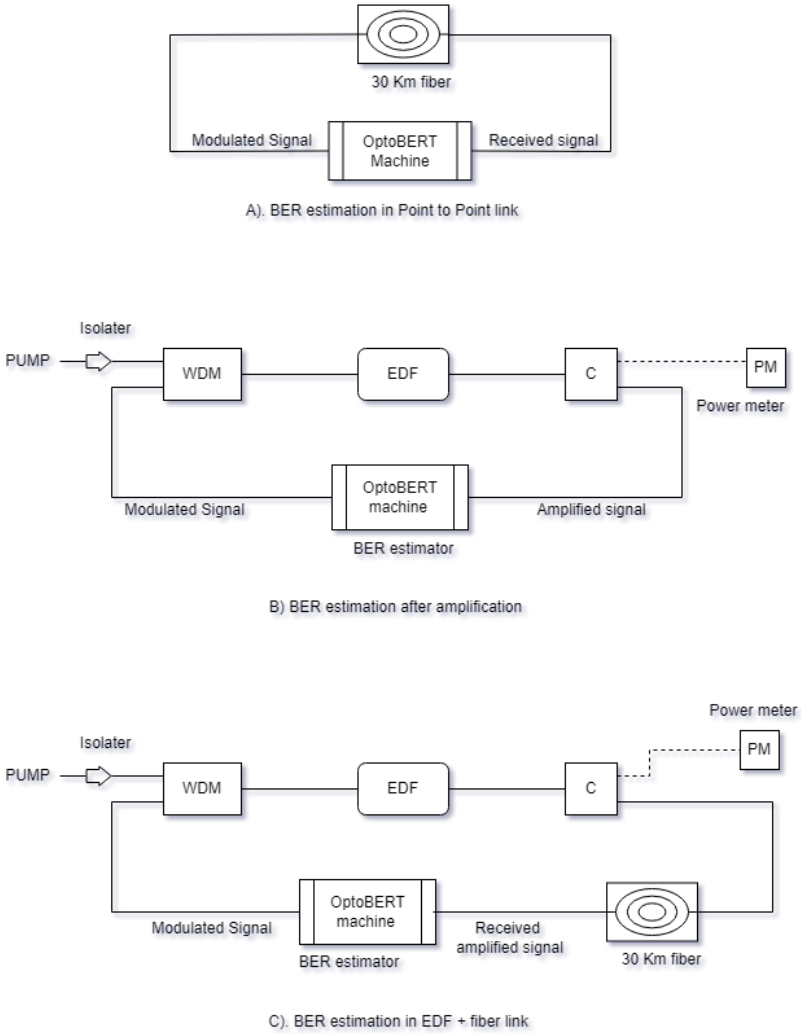

Figure 5.1: Schemes for estimation effect of amplification due to EDF on BER

Sequence	Pump Power	BER
PRBS7	C100	3.33E-12
	C150	3.01E-08
PRBS31	C100	0.00E+00
	C150	2.03E-08
1010 1010... 32bit seq	C100	8.50E-11
	C150	1.46E-08
1100 1100 ... 32bit seq	C100	5.07E-10
	C150	2.67E-08

Table 5.2: BER measurement for amplification by EDFA plus 30 km fiber link

Modulated signal @ 10Gbps	BER
PRBS7	7.04E-05
PRBS31	2.34E-05
1010 1010 ...user pattern	8.12E-10
1100 1100 ...user pattern	0.00E+00

Table 5.3: BER analysis of 30 km fiber link

APPENDIX A

SATURABLE ABSORBER MIRROR (SAM)

A.1 AIM

To determine the reflectance curve of SAM at λ = 980 nm pump wavelength.

A.2 SAM-1550-7-10PS DATA

A.2.1 Main SAM data

Laser wavelength	λ = 1550 nm
Absorbance	A = 7 % at 1550 nm
Saturation fluence	ϕ_{sat} = 15 $\mu J/m^2$
Relaxation time	τ = 10 ps
Damage threshold	ϕ = 800 $\mu J/m^2$

A.2.2 Reflectance Spectra

SAM has a well shaped low intensity reflectance spectra in the wavelength window 1450-1580 nm. It returns minimum power at 1518 nm where reflection is just below 75% and the rest gets absorbed in the absorber layerv (see Fig. A.1). On the contrary, for a pulsed input, the reflectance spectra of the SAM as a function of the incident fluence is shown in Fig. A.2.

Here we are carrying out the following two experiments for SAM reflectance characterization. First we use a TLS and look at the CW low intnesity reflectance as a function of the wavelength. In the next experiment we use pulsed 1550 nm light and launch it on the SAM and measure its reflectance. We change the fluence by changing the on time of the generated pulse.

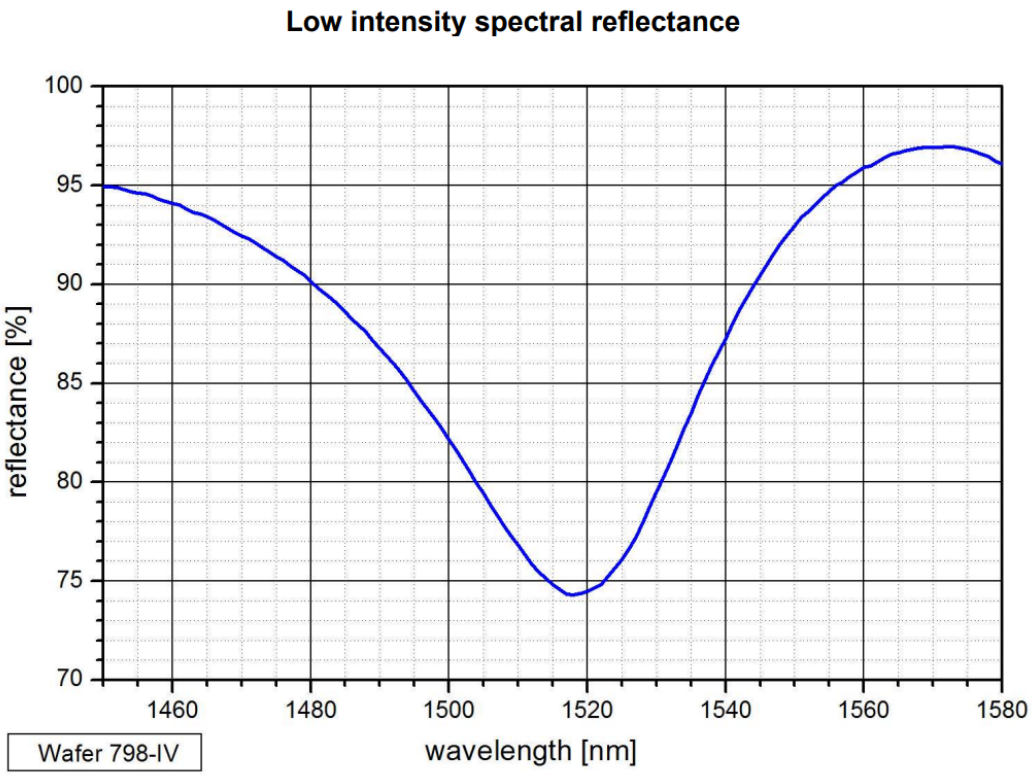

Figure A.1: Low intensity reflectance spectra of SAM as a function of the incident wavelength from Dataset

A.3 THEORY

A.3.1 What is SAM

The saturable absorber mirror (SAM) serves as nonlinear optical device to start and maintain continuous wave (cw) mode-locking.

A.3.2 Working Principle

The SAM consists of a mirror for the laser wavelength and an absorber layer in front of this mirror. The reflectance R = 1 - A of the SAM is determined by the absorption A of the absorber layer alone since the transmission though the mirror is negligible. The absorber layer contain a thin layers of a semiconductor material with band gap energy E_g slightly smaller then the photon energy hν of the laser light. Close to the band gap the density of states in the absorber is small and a few absorbed photons in each cycle can partially saturate the absorber which subsequently increases the SAM reflectance and

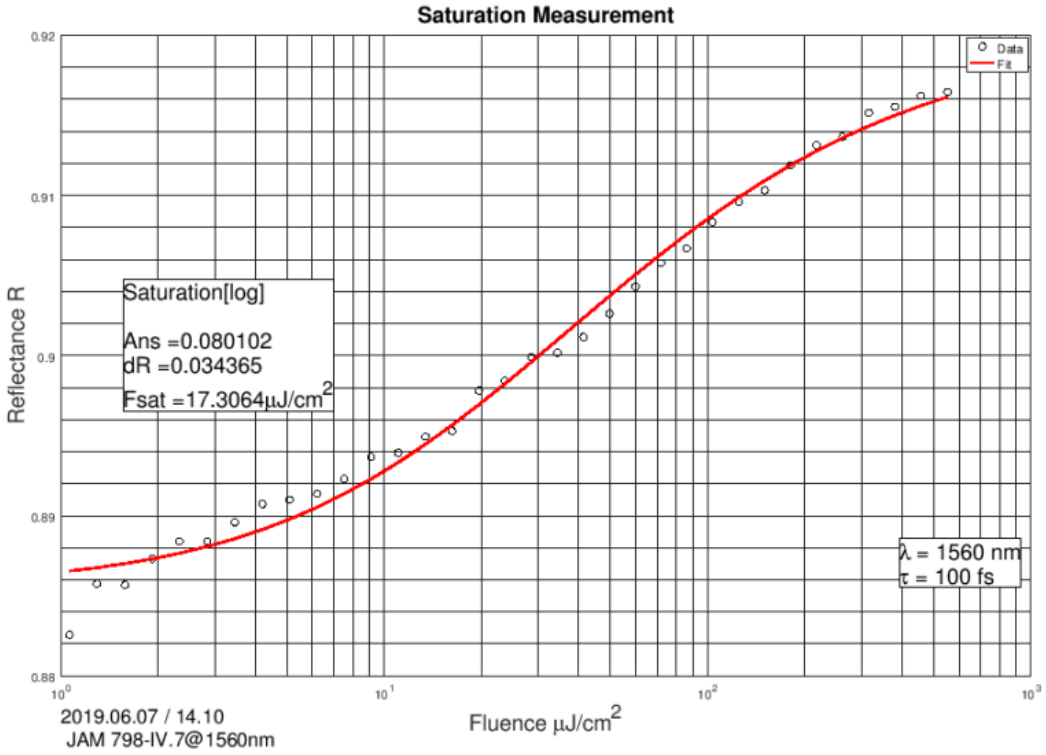

Figure A.2: Reflectance spectra of SAM as a function of input fluence from Dataset

therefore decrease the loss in the laser cavity.

A.4 EXPERIMENT SETUP

We generated pulsed laser source using cw light from TLS and modulated it with RF pulse(generated from AWG) with EOM, See fig A.3. We fed the generated pulsed light into edf, varried the pump power and went upto 700 $\mu J/cm^2$ fluence below the damage threshold of SAM which is 800 $\mu J/cm^2$ fluence. See table A.1 for noted data from the experiment. We tried the expt. with different pulse source like 16nm, 8nm and 4nm and observed the similar reflactance plot as shown in fig A.3.

A.5 RESULTS

We tried to get the reflactance characteristic curve of the SAM but didn't observe reflectance more than 1% at any input fluence to the SAM. It suggest either SAM is

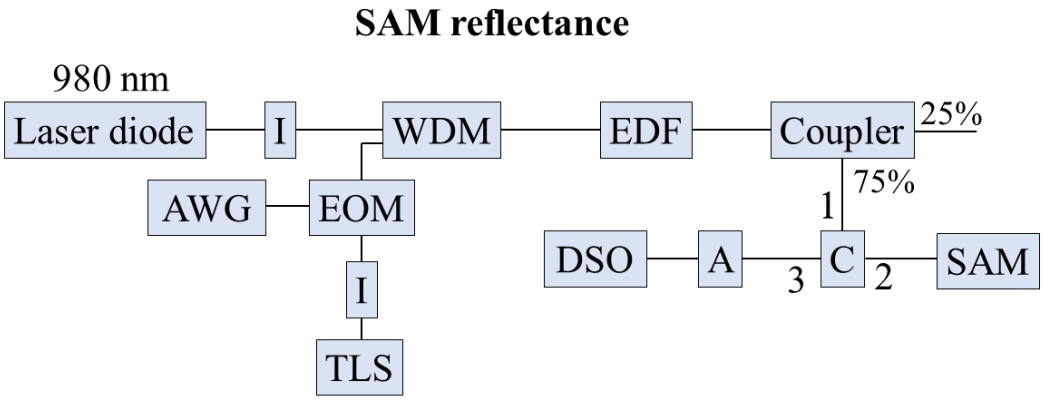

Figure A.3: Scheme used for characterising SAM reflactence with a pulsed input.

damaged entirely or at some parts.

Current(hex)	Current drawn(A)	IMON	5% of EDF output (dBm)	SAM output (dBm)
C000	0.05	0CD	$-\infty$	$-\infty$
C050	0.16	438	-4.2	-33.3
C090	0.26	438	1.2	-27.97
C130	0.49	430	6.5	-21.99
C150	0.53	434	7.5	-21.7
C190	0.63	41F	8.8	-21.02
C210	0.81	431	10.6	-20.19

Table A.1: SAM reflectance data collected from cw light input

A.6 CONCLUSION

From the experiments carried out to characterize the reflectance spectra of the SAM, we found out that both for CW input and pulsed input, the SAM showed a very low reflectance. This brings us to the conclusion that the SAM is not functioning as expected.

With hindsight of future experiments, we came to know that the SAM had a lot of dirt

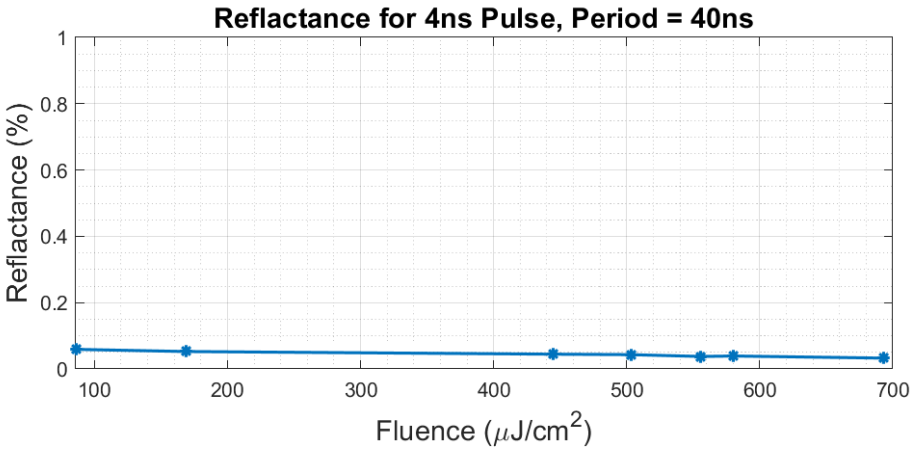

Figure A.4: Reflactance(%) of SAM with increasing fluence

Pump DAC	i/p (DSO reading, mV)	i/p (mW)	Fluence ($\mu J/cm^2$)	Ref. Power(DSO reading, mV)	Reflected Power(mW)	Reflectance (%)
40	47	9.4	44.3	0.0	0.00	0.00
50	91.5	18.3	86.2	0.5	0.01	0.06
70	179	35.8	168.7	0.9	0.02	0.05
100	472	94.4	444.7	2.1	0.04	0.04
120	534	106.8	503.1	2.3	0.05	0.04
150	590	118	555.9	2.2	0.04	0.04
170	616	123.2	580.4	2.4	0.05	0.04
200	736	147.2	693.5	2.4	0.05	0.03

Table A.2: Data collected experimentally to characterise SAM with increasing fluence

deposited on its surface, that eventually damaged its surface as well as the fiber tip it was connected to (see Fig. A.5).

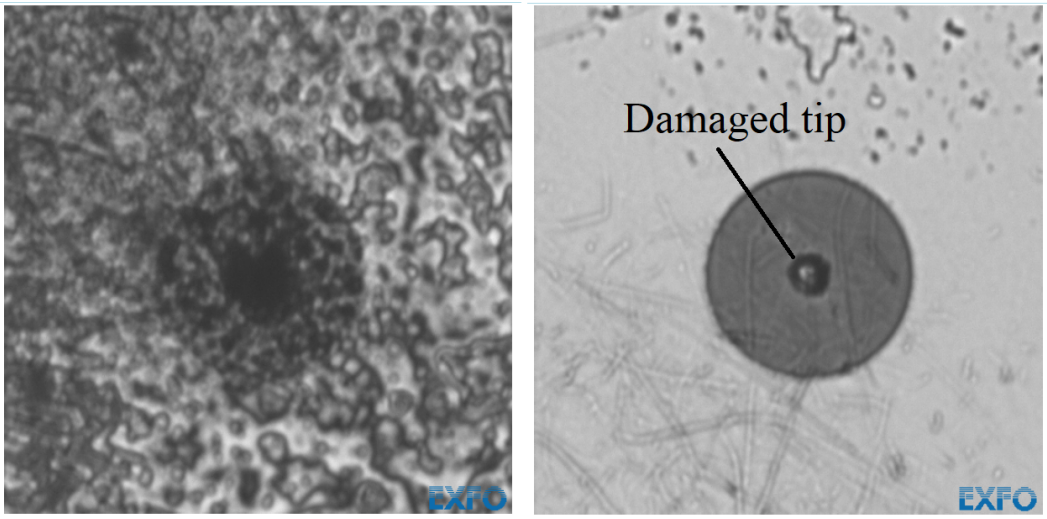

Figure A.5: SAM fiber tip before (left) and after (right) cleaning

APPENDIX B

CHARACTERISATION OF INBUILT PUMP CONNECTED TO EDF

B.1 PUMP CHARACTERIZATION

Above EDF being used is spliced to a 980 nm pump thru an isolator and WDM coupler, removing direct way of measuring the pump optical power going into the EDF. Thus throughout this discussion we will be using a conversion formula that converts current code(CXXX) into optical pump output power P_o in mW[1]. here D refers to the last three digits in CXXX. The relation between D, I and P_o are given by :

$$I = 1.789D - 52.348, \quad P_o = 0.7283I - 37.1359. \tag{B.1}$$

We can see negative pump power(see Fig. B.1) for DAC value below 060 which is

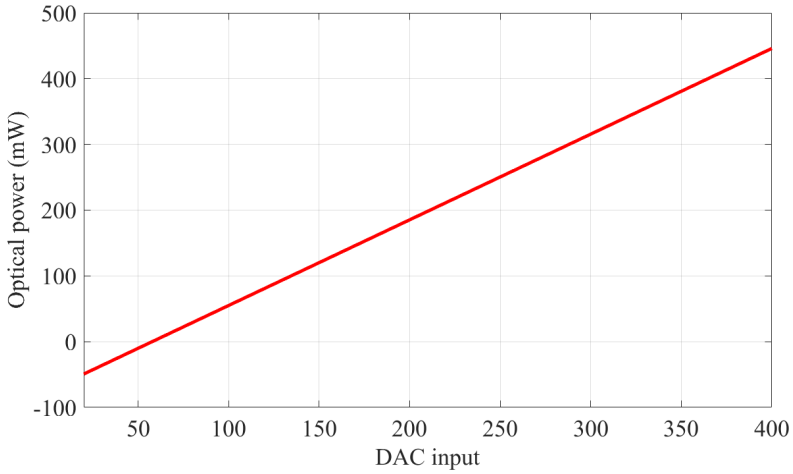

Figure B.1: Optical power of pump as a function of input DAC value.

physically impossible. Therefore the linear conversions in Eq. (B.1) are only valid when the DAC value D is above 060.

[1]This conversion relation was obtained from Ikram Khan's report titled "LDMv2-SN0753723", where he characterized the pump output.

APPENDIX C

CIRCULATOR AND COUPLER CHARACTERISATION

C.1 CIRCULATOR CHARACTERIZATION

Circulator is three port device and we know that the side that had only one port is port 2 (blue fiber), the port 1 and 3 (red fiber and white fiber) need to be confirmed. Thus we perform the following experiment as shown in Fig. C.1, to identify the ports. We could also determine the insertion losses from ports 1 to 2 and 2 to 3.

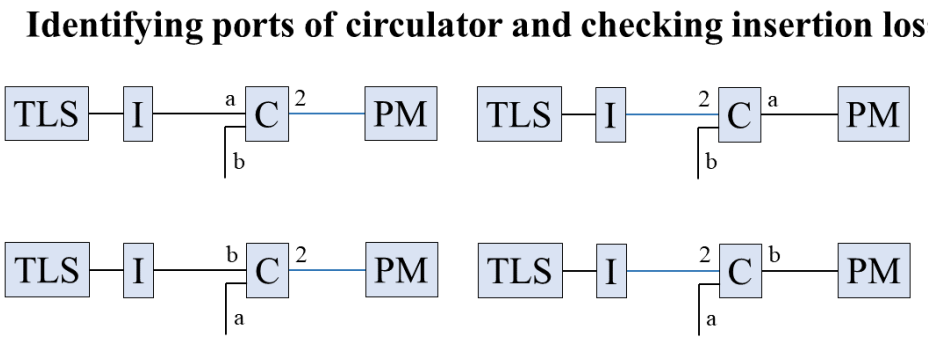

Figure C.1: Experimental schemes to identify the ports of a circulator. a and b are red and white ports respectively.

We measure the power after the isolator for all the cases shown in Fig. C.1 and it is found to be 3.68 dBm. For the different port configurations we measured the insertion loss. The insertion losses are tabulated in Table C.1. From Table C.1 it is evident that the port a (or red fiber) is port 1 and port b (or white fiber) is port 3 of the circulator.

C.2 COUPLER CHARACTERISATION

To find the coupling ratio of the 1×2 coupler that we want to use, we use the scheme

Input port	Output port	Insertion loss (dB)
a	2	1.2
2	a	> 50
b	2	> 50
2	b	0.7

Table C.1: Table for insertion loss at different ports of the circulator. (see Fig. C.1)

shown in Fig. C.2. Thus we launch a small signal (-6 dBm) into the EDF along with the

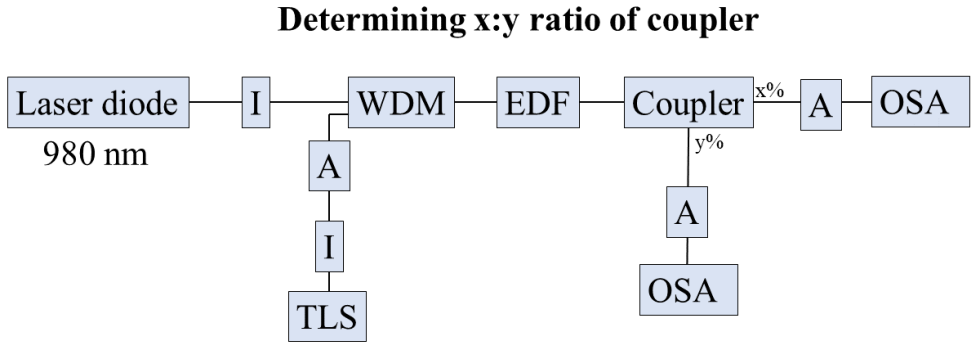

Figure C.2: Experimental scheme to find the coupling ratio of the 1×2 coupler.

pump (for different pump powers) and note the ratio of powers in the two output ports of the coupler. We found that the yellow colored coupler output port transmitted 24% power whereas the black colored coupler output port transmitted 76% power. Thus we conclude that it is a 75:25 coupler.

REFERENCES

1. **Chen, J.**, **X. Zhu**, and **W. Sibbett** (1992). Rate-equation studies of earbium-doped fiber lasers with common pump and laser energy bands. *J. Opt. Soc. Am. B*, **9**(10), 1876–1882. URL http://opg.optica.org/josab/abstract.cfm?URI=josab-9-10-1876.

2. **Keiser, G.**, *Optical Fiber Communications*. McGraw-Hill Publishing, 2010. ISBN 9780077418014. URL https://books.google.co.in/books?id=hGaEywEACAAJ.